NANO LETTERS

Letter

pubs.acs.org/NanoLett

3D Motion of DNA-Au Nanoconjugates in Graphene Liquid Cell Electron Microscopy

Qian Chen,[†,‡,∥] Jessica M. Smith,[†,‡] Jungwon Park,[†,‡] Kwanpyo Kim,[‡,§] Davy Ho,[†] Haider I. Rasool,[‡,§] Alex Zettl,[‡,§] and A. Paul Alivisatos*[,†,‡]

[†]Department of Chemistry, [∥]Miller Institute for Basic Research in Science, and [§]Department of Physics, University of California, Berkeley, California 94720, United States

[‡]Materials Sciences Division, Lawrence Berkeley National Laboratory, Berkeley, California 94720, United States

Supporting Information

ABSTRACT: Liquid-phase transmission electron microscopy (TEM) can probe and visualize dynamic events with structural or functional details at the nanoscale in a liquid medium. Earlier efforts have focused on the growth and transformation kinetics of hard material systems, relying on their stability under electron beam. Our recently developed graphene liquid cell technique pushed the spatial resolution of such imaging to the atomic scale but still focused on growth trajectories of metallic nanocrystals. Here, we adopt this technique to imaging three-dimensional (3D) dynamics of soft materials instead, double strand (dsDNA) connecting Au nanocrystals as one example, at nanometer resolution. We demonstrate first that a graphene liquid cell can seal an aqueous sample solution of a lower vapor pressure than previously investigated well against the high vacuum in TEM. Then, from quantitative analysis of real time nanocrystal trajectories, we show that the status and configuration of dsDNA dictate the motions of linked nanocrystals throughout the imaging time of minutes. This sustained connecting ability of dsDNA enables this unprecedented continuous imaging of its dynamics via TEM. Furthermore, the inert graphene surface minimizes sample−substrate interaction and allows the whole nanostructure to rotate freely in the liquid environment; we thus develop and implement the reconstruction of 3D configuration and motions of the nanostructure from the series of 2D projected TEM images captured while it rotates. In addition to further proving the nanoconjugate structural stability, this reconstruction demonstrates 3D dynamic imaging by TEM beyond its conventional use in seeing a flattened and dry sample. Altogether, we foresee the new and exciting use of graphene liquid cell TEM in imaging 3D biomolecular transformations or interaction dynamics at nanometer resolution.

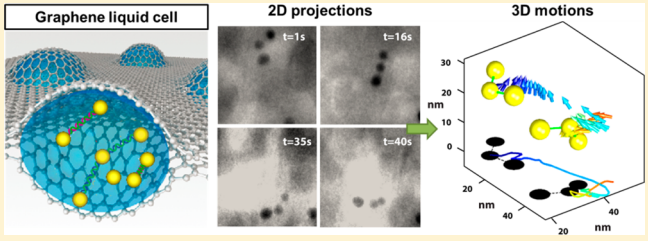

KEYWORDS: *3D motion, graphene liquid cell TEM, DNA nanotechnology*

A significant challenge in microscopy has been to visualize the dynamics of soft materials, in particular biological systems,[1−7] at the nanoscale to confirm or extend the extensive insights predicted by molecular theory and simulation.[8−10] One strategy followed in the electron microscopy community is to obtain high spatial resolution "snapshots" from distinct members of an ensemble of artificially fixated samples in their native liquid environment, each sample exhibiting one stage in a dynamic process.[2,5] Later these snapshots are assigned by the observer to a proposed sequence and then merged into a continuous dynamic movie. Transmission electron microscopy (TEM) achieves highly resolved structural details from the laborious sample preparations of a system frozen in vitrified ice,[2] which provides little information about a real continuous dynamic trajectory since the observations are derived from separate stationary and fixated samples. Super resolution optical microscopy can either obtain such stationary "snapshots" or continuous frames of images with a record resolution of ∼15 nm,[4,7] but for solely the spatial distribution, not structural and morphology details. Emerging liquid cell TEM techniques[11−20] have the potential to capture dynamic events in real time by interfacing ultrathin specimens in their native liquid phase with the high-resolution capabilities of EM. Previous studies using different versions of such liquid cells have not yet provided a real time trajectory of aqueous biomolecules due to many challenges:[1−5] the poor contrast of the low atomic number elements abundant in biological samples, the sensitivity to radiation damage, and the leaking of low vapor pressure solvent from the liquid cells. Because of these challenges, previous studies of biological systems using different versions of these liquid cells emphasize maintaining a hydrated environment during the imaging.[21−28]

Here we use a novel graphene liquid cell for transmission electron microscopy recently developed in this laboratory.[12] The unique design and material property of the graphene liquid cell[12,27,29] promise to tackle the previously identified challenges. The single atom thick graphene layer, the strongest and thinnest possible membrane, minimizes unwanted loss of the

Received: July 21, 2013
Published: August 14, 2013

Scheme 1. Graphene Liquid Cell Imaging of Au Nanocrystal-dsDNA Nanoconjugates: (A) Schematic of a Graphene Liquid Cell with Multiple Liquid Pockets, Containing Single Nanoparticles, Dimers Composed of dsDNA Bridges in Different Lengths, and Trimers, (B) Schematic of a Dimer and Its Projection as Two Dark Circular Shapes onto a Planar TEM Imaging Surface, and (C) TEM Images (Center Positions Aligned) of a Rotating Dimer[a]

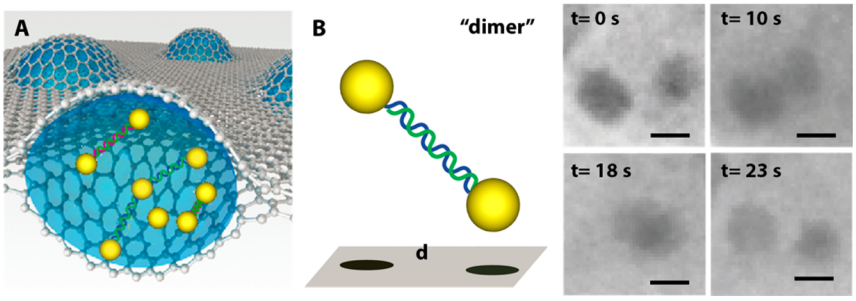

[a]At t = 18 s, the projections of two Au nanoparticles overlap with each other, indicating the dimer is almost perpendicular to the viewing screen (see Video S1). The scale bar is 5 nm.

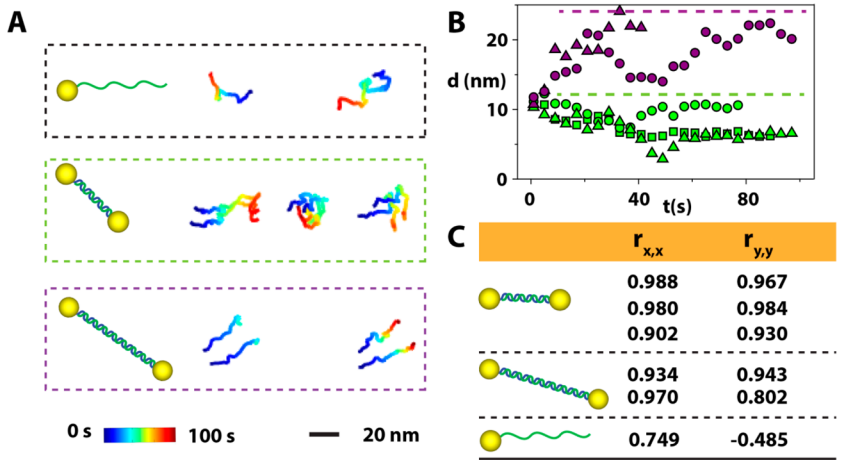

Figure 1. A collection of Au nanocrystal trajectories in the same liquid pocket. (A) An overview of the different trajectories color coded with time: individual particles (boxed in black), dimers linked by 42 base pair dsDNA (boxed in green), and dimers linked by 84 base pair dsDNA (boxed in purple). (B) The fluctuation of projected interparticle distance with time for three 42 bp dimers (green data points) and two 84 bp dimers (purple data points). The dotted lines highlight the maxima of interparticle distances. (C) A table of the Pearson's correlation coefficients showing the degree of linear correlation of x ($r_{x,x}$) and y ($r_{y,y}$) components of two trajectories.

imaging electrons by a window material and provides superior contrast and resolution compared to the conventional Si_3N_4 windows used in other liquid cell techniques.[12] In the graphene liquid cell, a pocket of approximately 100 nm peak height[12] and 1 μm diameter (see Figure S1) is trapped between two extended graphene sheets which are bonded to each other by their van der Waals attraction in the region where the liquid is not trapped. Unlike the artificial adhesion from the spacers in other liquid cells,[13−21] this strong native attraction minimizes potential contaminations and leakage during sample preparation procedures. The high electron and thermal conductivities of graphene enable fast transfer of accumulated charges or heat from electron beam, so this is a promising system to lower radiation damage to a biological sample. Note that this experiment can be done on a conventional TEM microscope without modification or customization of the TEM itself or the TEM holder.

We choose to study real-time dynamics of dsDNA conjugated with Au nanocrystals using a graphene liquid cell TEM for two reasons (see Scheme 1). Au-DNA nanoconjugates have been widely used as dynamic plasmonic probes[30−32] correlating an optical shift to a change in configuration due to a localized environmental stimulus. The direct imaging of their 3D configuration and the transformative process will enable on-demand design of such assembled sensors. This DNA assembled nanostructure incorporates both a biological molecule (the linker dsDNA) and a hard inorganic material (the high contrast Au nanocrystal) in TEM imaging. The presence of dsDNA molecules incorporates the major challenges of studying the dynamics of biological samples with TEM and in our experiment demonstrates the potential of the graphene liquid cell technique for studying the dynamics of biological samples with liquid-phase TEM. The high-contrast Au nanocrystals, on the other hand, facilitate tracking of our specimens. In addition, their motions at the single particle level shown below allow us to infer the configuration and status of DNA molecules under the electron beam. In particular, we observe dimers (pairs of gold nanoparticles tethered by a single piece of dsDNA) and trimers (three gold nanoparticles connected into a linear configuration by two single dsDNA bridges) as shown in Scheme 1A.

In our previous report of graphene liquid cell EM,[12] we encapsulated an ultrathin layer of organic nanocrystal growth solution and achieved ultrahigh resolution of in situ Pt nanocrystal growth TEM imaging. Here, we use an aqueous solution which is more evaporative. The strong van der Waals

dx.doi.org/10.1021/nl402694n | Nano Lett. 2013, 13, 4556−4561

attraction between two graphene membranes successfully seals specimens in the aqueous phase while the capillary force induced by its evaporation brings the top and bottom graphene layers in conformal contact. Stable aqueous solution pockets around one micrometer in size are rendered from this sealing mechanism, allowing for continuous imaging of the motion dynamics up to 2 min (see Figure S1) when exposed to the imaging electron beam accelerated by 200 kV.

The moving Au-dsDNA nanoconjugates in liquid are captured, under optimized imaging conditions (see Materials and Methods in the Supporting Information), as clusters of dark circular shapes projected onto the camera mounted in the TEM. For example, as shown in Scheme 1B,C and Video S1, the projections of two component Au nanocrystals of a dimer fluctuate in their distance; at certain instances, they even overlap and then diffuse slightly apart (Scheme 1C). The transient overlapping of two close nanocrystals indicates that the 3D rotation of the dimer is a significant component in the fluctuation of the distances between projections of particles in addition to a possible contribution from the linker DNA length fluctuation. This 3D rotation of the dimer demonstrates the thickness of the liquid pockets allows sufficient space for such rotation of 20 nm size clusters, and the graphene membrane does not perturb dynamics of Au-dsDNA conjugates by substrate−nanocrystal attraction. It is noteworthy that localized substrate attractions with nanocrystal from other types of window materials such as Si_3N_4[17] have confined the particle motion in liquid and render little observation of 3D dynamics.

First, we observed the motion of various types of Au-dsDNA conjugates, in the same liquid pocket to maintain the same physical condition for reliable quantitative analysis. The liquid pocket encapsulates differently designed configurations: Au-single strand DNA, short Au-dsDNA-Au (42 base pair DNA), and long Au-dsDNA-Au (84 base pair DNA), resulting in different dynamic features. Figure 1A shows a collection of 2D projected trajectories for those nanoconjugates in one liquid pocket color scaled according to elapsed time. Trajectories of free and single Au nanoparticles are visually distinguishable from clusters of two roughly parallel trajectories.

A series of quantitative analysis of the clustered trajectories indicates that the dsDNA linkers remain holding adjacent nanocrystals over prolonged periods of imaging time. First, the projected interparticle distances, though fluctuating, are consistently measured to be smaller than the estimated length of bridging dsDNA linkers (12 nm for 42 bp DNA) over 100 s (see green dots in Figure 1B). In comparison, in the same liquid pocket with the same liquid environment, free Au nanoparticles not connecting to adjacent particles are measured to have a diffusivity of 1.7 nm^2/s (see Figure 2B) and thus can diffuse 25 nm on average during 100 s, much larger than the linker length. Second, the projected interparticle distance between Au nanocrystals fluctuates in a dimension determined by the length of dsDNA bridges (see Figure 1B, 42 bp in green, 84 bp in purple). Not only do the projected interparticle distances from independent trajectories in each group exhibit the same maximum value, the maximum value of the 42 bp sample is also consistently half of that of the 84 bp one. The consistency between the linker length and observed interparticle distance demonstrates the structural integrity of the dsDNA in the dimer throughout the observation period. Third, the Pearson's correlation coefficients (defined as $r_{a,b} = \{[\sum_{i=1}^{n}(a_i - \bar{a})(b_i - \bar{b})]/[\sum_{i=1}^{n}(a_i - \bar{a})^2\sum_{i=1}^{n}(b_i - \bar{b})^2]^{1/2}\}$ for vectors a, b of the same dimension) for the x ($r_{x,x}$) and y ($r_{y,y}$) components

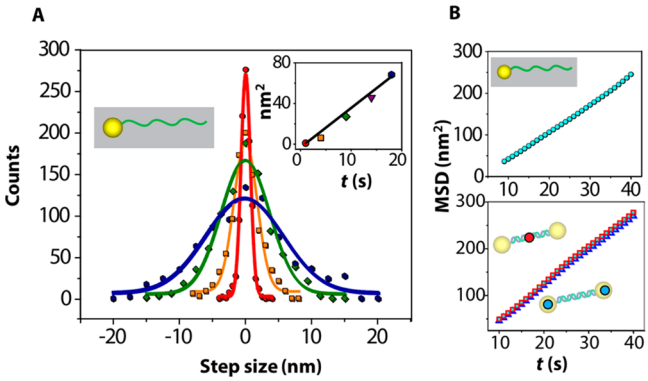

Figure 2. Diffusional statistics of Au-single strand DNA and Au-42 bp dsDNA trajectories. (A) Step size, i.e., diffusional displacement, distribution of ensemble averaged single particle trajectories for different time "steps": red circles for 1 s, orange squares for 4 s, green diamonds for 9 s, and blue hexagons for 18 s. The connecting lines, with the same coloring theme, are the Gaussian fittings. The inset shows the linear relationship between the fitted Gaussian widths for each curve with time. (B) The MSD−t plot for single particles (above) and dimers (below). In the plot for dimers, we show two ways of describing its motion, center-of-mass of the dimer (red squares), and ends of the dimer (blue triangles).

of each clustered pair of trajectories all show a high positive correlation, but low or even negative correlation for that of two free particles (see Figure 1C). These three features were reproduced across many samples of nanoconjugates. Taken together, the observations described here indicate that bridging dsDNA are able to hold the component nanocrystal of the nanoconjugates during the imaging process.

Earlier reports show that short dsDNA attached to gold nanoparticles can still fluctuate below its persistence length of around 50 nm due to the flexibility of the DNA.[33] Here we look into the nature of diffusional statistics of the Au nanocrystal trajectories, since the projected interparticle distance alone is complicated by nanoconjugate rotations. The bridge length between the dimers is shown to be regarded constant or its fluctuation not differentiable within our resolved temporal window (1 frame per second).

The diffusional dynamics of both dimers and free nanocrystals are compared for trajectories observed in the same liquid pocket. The mean square displacement (MSD = $\langle|\boldsymbol{r}(t) - \boldsymbol{r}(0)|^2\rangle$) and diffusion time t are calculated from ensemble average of all the trajectories. A linear relationship between MSD and diffusion time t, indicating Brownian diffusion (MSD = $4Dt$), is found for both single particle and dimer trajectories as shown in Figure 2B. Interestingly, the diffusivity D, one-fourth of the measured MSD−t curve slope, are the same for single particles and dimers tracked by either center-of-mass or end motions. This convergence in diffusivities can be explained by modeling a dimer as two single particles connected by an elastic spring, which relaxes at a time scale much faster than our observation time scale so as to smear out possible constraints in motion felt by the two component particles (see further discussion in Text S1). Thus, we see a constant linker length from this averaging. The measured abnormally sluggish diffusivity D = 1.7 nm^2/s agrees with values determined in previous reports on slowed nanocrystal diffusions[12,16,17] in various liquid cell configurations (see Table S1). More importantly, this slowed motion in a liquid cell configuration allows observation of nanoscale objects within the instrument

dx.doi.org/10.1021/nl402694n | Nano Lett. 2013, 13, 4556−4561

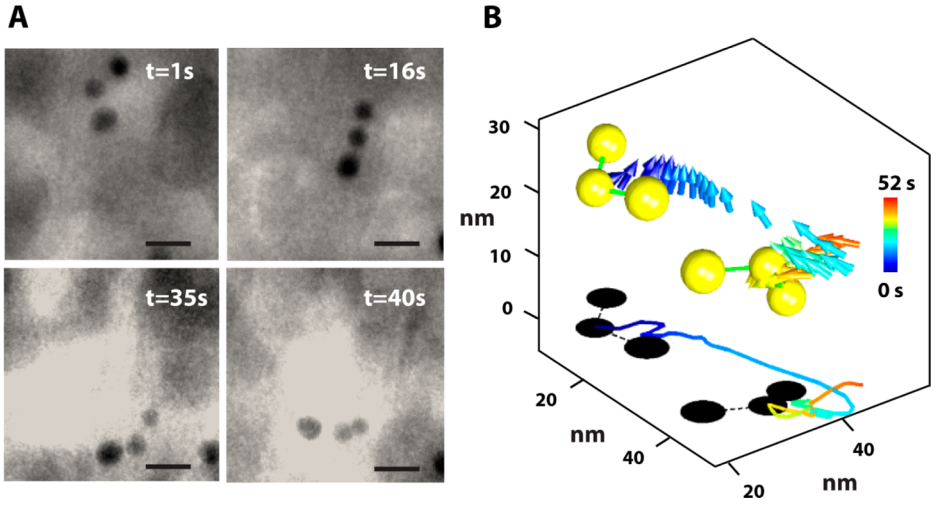

Figure 3. The 3D configuration and motion of a trimer. (A) Time-elapsed TEM images of a trimer with viewing position fixed. The background fluctuation due to the liquid is in position with previous liquid cell TEM studies. (B) The reconstructed rotational (color coded arrows) and translational (color coded dots for the central nanocrystal) motion of the trimer in three dimensions. The two representative 3D trimers (yellow spheres linked by green lines) show their configuration as well as configuration at t = 1 s and 40 s, respectively. See Video S2 for synchronized TEM and reconstruction series. Their projections (black circular shapes) match with TEM images well. The scale bar is 10 nm.

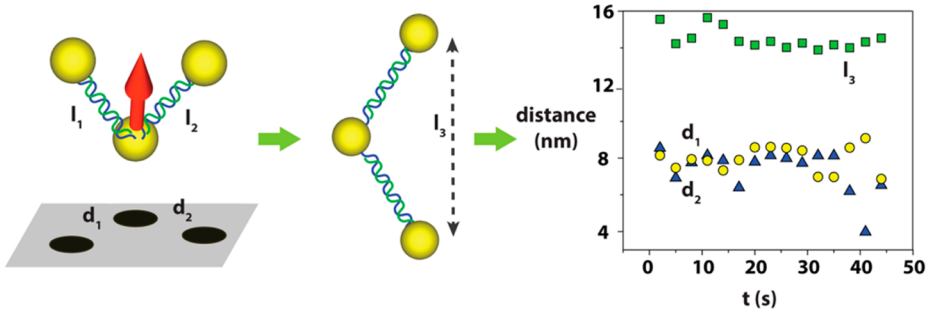

Figure 4. Iterative construction for the trimer shown in Figure 3. From left to right: a trimer in a 3D space, with interparticle linker lengths l_1 and l_2, and red arrow showing its orientation. For each frame one trimer is reconstructed with l_3. l_3 (green squares) remains constant throughout the 42 s of observation time, while the projected interparticle distances d_1 and d_2 fluctuate significantly more due to rotation.

capability; in contrast, these objects, if suspended in a bulk environment, exhibit ultrafast Brownian diffusion that overwhelms data collection capability.

It is also inferred from another statistical measure, the step-size distribution of ensemble free nanocrystal trajectories, that no localized attraction between the nanocrystal and the substrate is observed. The single Gaussian shape of the distribution (Figure 2A) contrasts with the multiple Gaussians in Si_3N_4 liquid cell studies[17] and echoes our observation of a rotating dimer (Scheme 1C). Evidently, the force of attraction between the nanocrystals and the graphene is much smaller than with the silicon nitride, so that the graphene does not perturb the trajectories, while the silicon nitride does. The width of the Gaussian is linearly related to step size, which in return demonstrates the Brownian nature of the particle motions in this liquid pocket, the basis for our comparative study above (see inset of Figure 2A).

Now that we have demonstrated that nanoconjugates rotate freely with structural rigidity in the liquid pocket, we extract the configuration and motion of dsDNA-Au nanoconjugates in three dimensions from time-elapsed TEM images. Such information, though critical to their plasmonic coupled properties,[30,31] has been previously inaccessible from conventional TEM because drying samples on a grid flattens any 3D structure through evaporation. Our frame-based iterative optimization method does not require a priori knowledge of the linker lengths but uses reasonably arbitrary values as initial numbers. These initially assigned linker lengths are iterated until they converge toward one rigid structure in three dimensions for all of the frames in the continuous trajectory.

Figure 3 demonstrates the validity of this iterative method: from the raw TEM images (Figure 3A), both the rotational (color-coded arrows) and translational (color-coded dots) motions are as shown in Figure 3B, reestablished from one converged 3D trimer structure. We use a trimer to show how our iterative reconstruction works, but the principles we introduce here can be applied extensively to other types of 3D frameworks. The iteration starts from a set of linker lengths, l_1 and l_2 (Figure 4). The ratio between the linker length $l_{1,2}$ and projected length $d_{1,2}$ generates the z coordinates, while the projected positions read x and y coordinates directly. Each frame thus generates one set of 3D positions for each particle, that is, 3D configuration of the trimer. The iteration continues, with the inputs being adaptive, until the trimers constructed from all the frames, continuous yet independent from each other, converge into one structure (see Table S2). Mathematically, we use the standard deviation of the interparticle distance l_3 calculated from the obtained 3D coordinates of the trimer in each frame as the handle to finetune the initial values. The final set of l_1 and l_2 values are obtained after the calculated standard

dx.doi.org/10.1021/nl402694n | Nano Lett. 2013, 13, 4556−4561

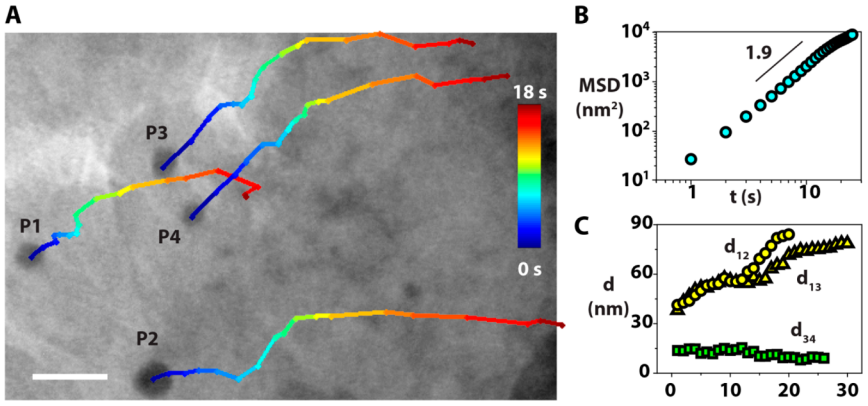

Figure 5. Motions of dimers and free single nanocrystals in a convection flow. (A) TEM images of four Au nanocrystals exhibiting superdiffusional motion. Colored traces are trajectories of each nanocrystal coded according to time. (B) The MSD−t plot on the log−log scale shows a power law coefficient of 1.9: MSD ~ $t^{1.9}$, indicating a non-Brownian, highly directional motion often as a result of solvent flow. (C) The projected interparticle distance with time. $d_{i,j}$ refers to the projected distance between particle i and particle j measured directly from the TEM images. While the projected distances between nonconnected Au nanocrystals increase with time (d_{12} and d_{13} in yellow), the projected distance between Au nanocrystals connected by dsDNA as a dimer fluctuates below the dsDNA length (d_{34} in green). The scale bar is 10 nm.

deviation of the set of l_3 is minimized, that is, after l_3 converges to a constant value for different image frames (see Figure 4). The final converged structure is now endowed with all degrees of freedom, following a four-dimensional trajectory matching with the continuous 2D movie we captured, as shown in Video S2. Here the principle of reconstructing 3D structure and motion from 2D projections is demonstrated, with details retrieved at high fidelity from a dynamic movie from liquid cell TEM. This principle and the technique can be easily extended to other structures in order to relate their 3D configuration and motions in solution to their function. One extension will be to image the 3D conformation dynamics of low contrast proteins using attached Au nanoparticles as high contrast agents.[23,26,28,34]

A surprising result here is the stability of the nanoconjugate structure composing of dsDNA linkers throughout the obesrvation under the electron microscope. The Au nanocrystal components of the nanoconjugates are retained for a prolonged time under an estimated dosage rate onto the graphene liquid cell as a whole: 60−100 $e^-/(Å^2 \cdot s)$ (see Text S2), which is more than the critical dosage previously reported for biological molecules.[4] Several observations from our experiment demonstrating the continued linking ability of the linkers are discussed above: the retention of the expected projected interparticle distance for a time far longer than that for which free particles would diffuse far apart (Figure 1b), the correlated motions in paired trajectories (Figure 1c), the rigid linker indicated from motion analysis (Figure 2), and the convergence of reconstructed structure into one single 3D configuration (Figures 3 and 4).

To further show nanoparticles are linked by dsDNA throughout the whole and the structural integrity of the nanoconjugate is conserved, we performed more experiments to confirm it based upon intentional manipulation via the electron beam. We focus the electron beam to induce huge convection or likely drill a hole in the liquid pocket membrane. All of the particles, no matter whether they are originally bridged by dsDNA or not, now move toward one direction, as the random Brownian motion is overwhelmed by solvent-driven convection (see Figure 5A). This directional, or superdiffusional, motion can be seen clearly from the MSD−t curve with a slope of 1.9 (see Figure 5B). Still dimers (see Figure 5C) differentiate themselves from single particles by maintaining a small interparticle distance during the violent convection process (see Figure 5 and Video S3).

The DNA linkers are vulnerable to the electron beam when the radiation exceeds manageable dosages. In the experiments when we exposed sample to the electron beam continuously over a prolonged imaging time, particles originally clustered and moving together are sometimes swept apart at a later time (Video S4), which in turn indicates that the linker has suddenly been broken.

We are aware that it is still an open question whether the existence of bridging linkers between Au nanocrystals corresponds to complete structural integrity of dsDNA in molecular level and how the graphene wrap together with liquid environment strive to stabilize dsDNA. More quantitative and comparative evaluation of radiation damage for a graphene liquid cell EM and normal EM is required and currently in progress. But the experimental facts promise dynamic trajectories including both position and 3D configurations for nanoconjugates and, in the future, biological molecules brought by graphene liquid cell.

Conclusions. We show the in situ observation of 3D dynamics of nanocrystal-DNA nanoconjugates, and we develop the 3D reconstruction of both the configuration and motions, which are inaccessible with a conventional TEM technique. Looking forward, this work opens many opportunities to study the dynamics of biological macromolecular assemblies and artificial nanostructures as they evolve and function in time.

■ ASSOCIATED CONTENT

Ⓢ Supporting Information

Text sections S1−S3, Figure S1, Table S1−S2, and Videos S1−S4. This material is available free of charge via the Internet at http://pubs.acs.org.

■ AUTHOR INFORMATION

Corresponding Author

*E-mail: apalivisatos@lbl.gov.

Present Addresses

J.P.: School of Engineering and Applied Sciences, Harvard University, Cambridge, Massachusetts 02138, United States.

K.K.: Department of Chemical Engineering, Stanford University, Stanford, California 94305, United States.

Notes

The authors declare no competing financial interest.

■ ACKNOWLEDGMENTS

We thank Peter Ercius at National Center for Electron Microscopy and David Chandler at UC Berkeley for useful discussions. This research was supported in part by the Defense Threat Reduction Agency (DTRA) under award HDTRA1-13-1-0035, which provided for in situ TEM experiments, as well as DNA-Au nanoparticle sample preparation; by the National Science Foundation within the Center of Integrated Nanomechanical Systems, under Grant EEC-0832819, which provided for early development of graphene lamination methods. Q.C. was supported by a Miller fellowship from Miller Institute for Basic Research in Science at UC Berkeley. J.S. was supported by Agilent Technologies Applications and Core Technology University Research Grant.

■ ABBREVIATIONS

TEM, transmission electron microscope; dsDNA, double-stranded DNA; 3D, three-dimensional

■ REFERENCES

(1) Evans, J. E.; Browning, N. D. *J. Electron Microsc. (Tokyo)* **2013**, *62*, 147−156.
(2) Kourkoutis, L. F.; Plitzko, J. M.; Baumeister, W. *Annu. Rev. Mater. Res.* **2012**, *42*, 33−58.
(3) Hui, S. W.; Parsons, D. F. *Science* **1974**, *184*, 77−78.
(4) Isaacson, M.; Johnson, D.; Crewe, A. V. *Radiat. Res.* **1973**, *55*, 205−224.
(5) Lorenz, U. J.; Zewail, A. H. *Proc. Natl. Acad. Sci. U.S.A.* **2013**, *110*, 2822−2827.
(6) Xu, K.; Zhong, G.; Zhuang, X. *Science* **2013**, *339*, 452−456.
(7) Jones, S. A.; Shim, S.-H.; He, J.; Zhuang, X. *Nat. Methods* **2011**, *8*, 499−508.
(8) Warshel, A.; Parson, W. W. *Q. Rev. Biophys.* **2001**, *34*, 563−678.
(9) Berendsen, H. J. C.; Hayward, S. *Curr. Opin. Struct. Biol.* **2000**, *10*, 165−169.
(10) Onuchic, J. N.; Wolynes, P. G. *Curr. Opin. Struct. Biol.* **2004**, *14*, 70−75.
(11) de Jonge, N.; Ross, F. M. *Nat. Nanotechnol.* **2011**, *6*, 695−704.
(12) Yuk, J. M.; et al. *Science* **2012**, *336*, 61−64.
(13) Li, D.; et al. *Science* **2012**, *336*, 1014−1018.
(14) Liao, H.-G.; Cui, L.; Whitelam, S.; Zheng, H. *Science* **2012**, *336*, 1011−1014.
(15) Radisic, A.; Ross, F. M.; Searson, P. C. *J. Phys. Chem. B* **2006**, *110*, 7862−7868.
(16) White, E. R.; Mecklenburg, M.; Shevitski, B.; Singer, S. B.; Regan, B. C. *Langmuir* **2012**, *28*, 3695−3698.
(17) Zheng, H.; Claridge, S. A.; Minor, A. M.; Alivisatos, A. P.; Dahmen, U. *Nano Lett.* **2009**, *9*, 2460−2465.
(18) Woehl, T. J.; Evans, J. E.; Arslan, I.; Ristenpart, W. D.; Browning, N. D. *ACS Nano* **2012**, *6*, 8599−8610.
(19) White, E. R.; et al. *ACS Nano* **2012**, *6*, 6308−6317.
(20) Evans, J. E.; Jungjohann, K. L.; Browning, N. D.; Arslan, I. *Nano Lett.* **2011**, *11*, 2809−2813.
(21) Mirsaidov, U. M.; Zheng, H.; Casana, Y.; Matsudaira, P. *Biophys. J.* **2012**, *102*, L15−L17.
(22) Peckys, D. B.; Mazur, P.; Gould, K. L.; de Jonge, N. *Biophys. J.* **2011**, *100*, 2522−2529.
(23) Peckys, D. B.; de Jonge, N. *Nano Lett.* **2011**, *11*, 1733−1738.
(24) Sugi, H.; et al. *Proc. Natl. Acad. Sci. U.S.A.* **2008**, *105*, 17396−17401.
(25) Liu, K.-L.; et al. *Lab Chip* **2008**, *8*, 1915−1921.
(26) Dukes, M. J.; Peckys, D. B.; de Jonge, N. *ACS Nano* **2010**, *4*, 4110−4116.
(27) Mohanty, N.; Fahrenholtz, M.; Nagaraja, A.; Boyle, D.; Berry, V. *Nano Lett.* **2011**, *11*, 1270−1275.
(28) Peckys, D. B.; de Jonge, N. *Nano Lett.* **2011**, *11*, 1733−1738.
(29) Krueger, M.; et al. *ACS Nano* **2011**, *5*, 10047−10054.
(30) Jun, Y. W.; Sheikholeslami, S.; Hostetter, D.; Tajon, C.; Craik, C.; Alivisatos, A. P. *Proc. Natl. Acad. Sci. U.S.A.* **2009**, *106*, 17735−17740.
(31) Liu, N.; Hentschel, M.; Weiss, T.; Alivisatos, A. P.; Giessen, H. *Science* **2011**, *332*, 1407−1410.
(32) Mastroianni, A. J.; Claridge, S. A.; Alivisatos, A. P. *J. Am. Chem. Soc.* **2009**, *131*, 8455−8459.
(33) Mastroianni, A. J.; Sivak, D. A.; Geissler, P. L.; Alivisatos, A. P. *Biophys. J.* **2009**, *97*, 1408−1417.
(34) Hu, M.; et al. *J. Struct. Biol.* **2008**, *161*, 83−91.